Engineering 3 (2017) 467–476

Contents lists available at ScienceDirect

Engineering

journal homepage: www.elsevier.com/locate/eng

Research
Clean Energy—Review

Particle Size and Crystal Phase Effects in Fischer-Tropsch Catalysts

Jin-Xun Liu[a], Peng Wang[a,b], Wayne Xu[b], Emiel J. M. Hensen[a,*]

[a] *Laboratory of Inorganic Materials Chemistry, Schuit Institute of Catalysis, Department of Chemical Engineering and Chemistry, Eindhoven University of Technology, Eindhoven 5600 MB, The Netherlands*
[b] *National Institute of Clean-and-Low-Carbon Energy, Beijing 102211, China*

ARTICLE INFO

Article history:
Received 14 March 2017
Revised 10 May 2017
Accepted 6 July 2017
Available online 14 August 2017

Keywords:
Fischer-Tropsch synthesis
Iron, cobalt, and ruthenium carbides
Size effect
Crystal structure

ABSTRACT

Fischer-Tropsch synthesis (FTS) is an increasingly important approach for producing liquid fuels and chemicals via syngas—that is, synthesis gas, a mixture of carbon monoxide and hydrogen—generated from coal, natural gas, or biomass. In FTS, dispersed transition metal nanoparticles are used to catalyze the reactions underlying the formation of carbon-carbon bonds. Catalytic activity and selectivity are strongly correlated with the electronic and geometric structure of the nanoparticles, which depend on the particle size, morphology, and crystallographic phase of the nanoparticles. In this article, we review recent works dealing with the aspects of bulk and surface sensitivity of the FTS reaction. Understanding the different catalytic behavior in more detail as a function of these parameters may guide the design of more active, selective, and stable FTS catalysts.

1. Introduction

Due to higher price levels of crude oil, Fischer-Tropsch synthesis (FTS), which converts coal, natural gas, and biomass to chemicals and liquid fuels, has attracted increasing attention in recent years as a way to diversify both the feedstock base for obtaining liquid transportation fuels and the monetization of natural gas and coal resources [1,2]. The principal reaction was discovered by Fischer and Tropsch [3] about 90 years ago. FTS reactions involve the strongly exothermic hydrogenation of carbon monoxide (CO) to paraffins and olefins according to the following chemical equations:

$$(2n+1)\,H_2 + nCO \longrightarrow C_nH_{2n+2} + nH_2O \quad (1)$$

$$2nH_2 + nCO \longrightarrow C_nH_{2n} + nH_2O \quad (2)$$

Aside from alkanes and alkenes, oxygenated hydrocarbons and carbon dioxide (CO_2) are obtained as by-products in industrial FTS. The mechanism underlying the FTS reaction is complex and involves many steps such as CO dissociation, carbon (C) hydrogenation, CH_x coupling reactions, and hydrogenation and dehydrogenation reactions that lead to hydrocarbon product desorption as well as oxygen (O) removal reactions [4]. There continues to be considerable debate about many of these steps, most notably the nature of the active site and the way CO is dissociated, which is closely linked to the question of which is the growth monomer in FTS. From a practical point of view, the main drivers for the improvement of FTS catalysts are higher activity, improved selectivity to targeted product classes such as long-chain hydrocarbons or light olefins, and improved lifetime.

In heterogeneous catalysis, it is well accepted that catalytic performance is governed by the electronic structure of the catalyst [5]. Tunable parameters are active phase composition, particle size, crystal structure, crystal morphology, and the formation of the interface between the transition metal nanoparticles and the support of the catalysts [6–11]. Typical transition metals for catalyzing the FTS reaction are ruthenium (Ru), cobalt (Co), and iron (Fe). All of these present high activity and selectivity toward liquid hydrocarbons in the low-temperature FTS reaction [12]. Although Ru is usually deemed to be too expensive for this purpose despite its high activity, Co and Fe

* Corresponding author.
E-mail address: E.J.M.Hensen@tue.nl

http://dx.doi.org/10.1016/J.ENG.2017.04.012

have been the main components of industrial FTS catalysts. Nickel (Ni)-based catalysts generally produce too much methane (CH_4) under practical reaction conditions [13]. Here, we review recent developments in the field of Co-, Ru-, and Fe-based catalysts for the production of alkanes, alkenes, and alcohols via the FTS process. The focus of this review is on the influence of particle size and crystal phase, in which catalyst synthesis, modern characterization techniques, and density functional theory calculations are playing increasingly important roles. This review consists of three main parts: first, a discussion of the particle size effects of Co-, Ru-, and Fe-based catalysts in FTS; second, a description of the crystal structure effect of Co, Ru, Fe, and Ni metals in FTS; and finally, conclusions and a brief perspective.

2. Particle size effect of FTS over Co-, Ru-, and Fe-based FTS catalysts

A general approach to increase catalytic activity is to improve the active phase surface area by decreasing the size of the particles that make up the active phase [7,11,14]. Increasing the number of exposed surface sites works well for structure-insensitive reactions [11]. However, many catalytic reactions are structure sensitive, implying that the specific activity depends on the dispersion in a more complex manner [7,11,15–17]. This becomes particularly evident when metal nanoparticles become smaller than 10 nm, as specific surface sites such as corners, edges, and step edges then become dominant over terrace sites. As the FTS reaction is a well-known structure-sensitive reaction, it is no wonder that many researchers have focused on resolving optimum particle size for high activity and selectivity. Given their importance in commercial operation, we limit our discussion of particle size effects to Co, Ru, and Fe nanoparticles.

2.1. Co particle size effect in FTS

Iglesia [18] showed that Co site-time yields are independent of Co particle size in the 10–210 nm range using aluminium oxide (Al_2O_3), silicon dioxide (SiO_2), and titanium dioxide (TiO_2) as supports. Bezemer et al. [15] contended that CO hydrogenation activity is insensitive when the (carbon-nanofiber-supported) Co nanoparticles are larger than 6 nm, but demonstrated that smaller Co nanoparticles (< 6 nm) have lower CO hydrogenation activity and higher CH_4 selectivity (Fig. 1). Steady-state isotopic transient kinetic analysis (SSITKA) measurements suggested that the lower CO consumption rates of small Co nanoparticles can be attributed to blocking of the active edge/corner sites by CO [7]. Higher hydrogen coverage on smaller particles explains the higher CH_4 selectivity that is observed for smaller Co nanoparticles. These trends have been confirmed by other groups for silica-supported Co catalysts [19,20]. An alternative interpretation offered is that smaller Co nanoparticles (< 2.5 nm) can be easily oxidized by water [19]. Different points of view on the effects of particle size may originate from different reaction conditions.

Herranz et al. [21] showed that Co nanoparticles remain metallic under methanation conditions. While CO methanation activity (i.e., the turnover frequency, TOF) of Co/SiO_2 catalysts decreases when particles become smaller than about 10 nm, the apparent activation energy for CO methanation is insensitive to Co particle size (Fig. 2). Hydrogen-deuterium exchange experiments indicate that the dissociation of H_2 is difficult on small Co nanoparticles, a reason that is used to explain lower rates for smaller particles. Further research provided evidence that CO activation is facilitated by the presence of hydrogen on Co nanoparticles, and that the ability to dissociate hydrogen is the key parameter determining FTS activity [22]. However, Holmen et al. [23] provided an alternative view on the Co particle size effect in FTS. Their SSITKA experiments showed that the number of surface CH_x intermediates increased with particle size, while the intrinsic activity remained constant when the Co particle size varied from 4 nm to 15 nm. They suggested that the site-based activity does not change in the 4–15 nm range, but that smaller particles have comparatively less active sites than larger ones.

Regarding FTS selectivity, quite small Co nanoparticles generally display increased CH_4 selectivity. There is a volcano-like curve for C_{5+} selectivity that varies with the particle size of $Co/\gamma\text{-}Al_2O_3$ catalysts, and the maximum selectivity was found for 7–8 nm Co nanoparticles [24]. This finding was confirmed by Holmen's [25] lateral work showing that the C_{5+} selectivity does indeed increase with Co particle size below 8–9 nm, and approaches a constant value for even larger Co particles. It is interesting that the lowest CH_4 selectivity as well as the highest olefin-to-paraffin ratio were obtained at maximum C_{5+} selectivity. Recently, Melaet et al. [26] found that the FTS reaction exhibited obvious changes with Co particle size (3.2–11 nm) in the product distribution at 250 °C. Fig. 3 shows that CH_4 selectivity increases with decreasing Co particle size, and is ac-

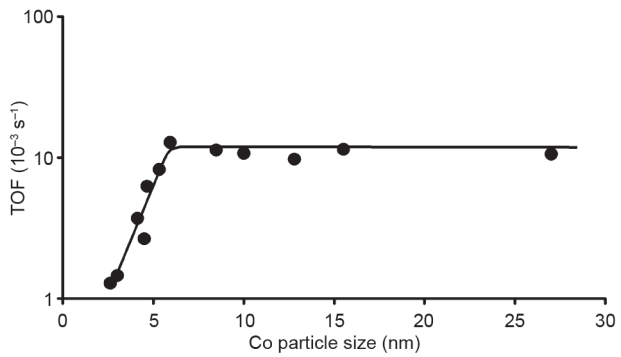

Fig. 1. Co particle size effect in the turnover frequency (TOF) of FTS (220 °C, $H_2/CO = 2$, 1 bar (1 bar = 10^5 Pa)) [15].

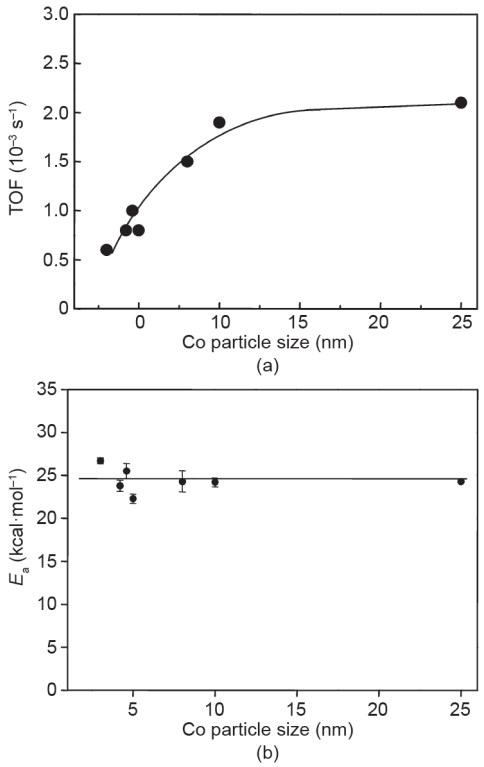

Fig. 2. CO methanation activity as a function of particle size. (a) TOF of CO hydrogenation at 240 °C; (b) activation energy (E_a) of CO hydrogenation varying with particle size [21]. 1 kcal = 4184 J.

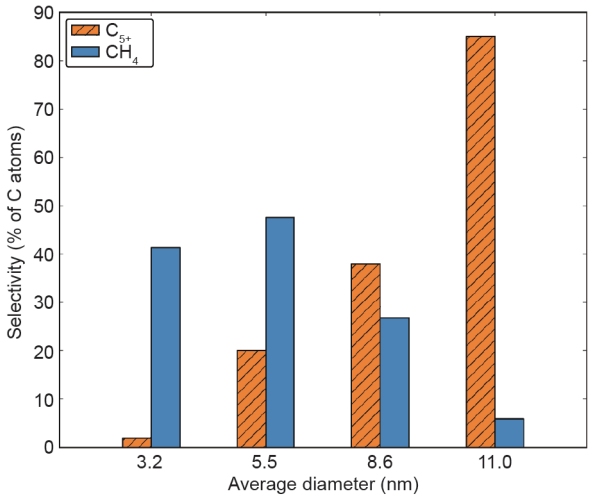

Fig. 3. Selectivities toward hydrocarbons (C_{5+} and CH_4) as a function of Co particle sizes for the CO hydrogenation reaction (250 °C, H_2/CO = 2, 5 bar). Both selectivities are calculated with respect to the total number of converted C atoms [26].

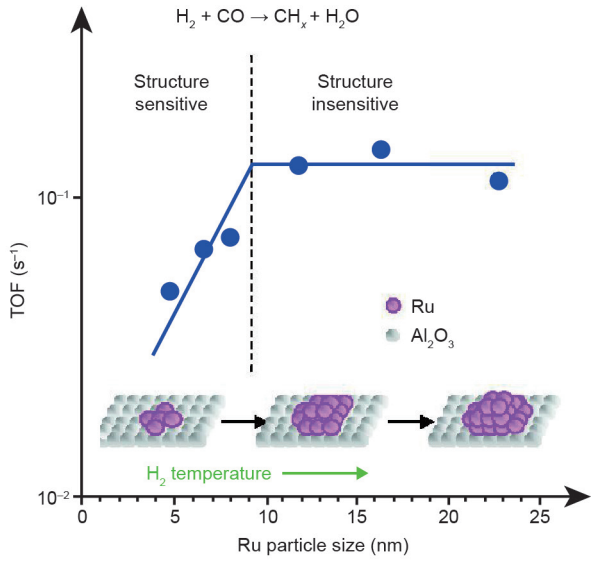

Fig. 4. CO consumption and CH_4 formation rates as a function of Ru particle size (523 K; 5.5 kPa CO, 55 kPa H_2, 124.5 kPa inert) [16].

companied by a decrease of the C_{5+} selectivity. This finding indicates that larger Co nanoparticles can produce longer hydrocarbon chains. However, the question of why larger Co nanoparticles produce longer hydrocarbon chains remains an open one.

2.2. Ru particle size effect in FTS

In the past, Dalla Betta et al. [27] and Iglesia et al. [28] reported that the intrinsic catalytic activity of a Ru-based catalyst for FTS reaction is not strongly dependent on the particle size. They proposed that the FTS reaction is structure insensitive. However, another two works reached the opposite conclusion—namely, that the specific activity is sensitive to Ru crystal size and metal dispersion [17,29]. The latter finding is supported by Kang's work [30], which showed that the TOF and product selectivities of the FTS reaction are strongly dependent on the particle size of the Ru-based catalyst. Carbon nanotube-supported Ru-based catalysts with a mean Ru particle size of ~7 nm display the highest activity and selectivity toward long-chain hydrocarbons. Xiao et al. [31] have developed Ru nanocluster catalysts that are used in aqueous-phase FTS. These Ru-based catalysts, which have a mean diameter of ~2 nm, presented extremely high activity under these anomalous conditions. Specifically, the FTS activity showed a dramatic increase when the particle size was reduced to 2 nm, with a smaller cluster exhibiting lower performance. Nevertheless, no clear explanation for Ru particle size effect has been advanced by these authors. However, our work showed that the small unsupported Ru nanoparticles have much lower FTS activity and exhibit an unprecedented oxygenate selectivity of 70% for aqueous-phase FTS under low-temperature conditions [32,33].

Carballo et al. [16] studied Ru/Al_2O_3 catalysts with different metal particle sizes and found that the TOF of the FTS reaction increases with Ru particle size, reaching a constant value for Ru nanoparticles larger than 10 nm; this is similar to what has been observed for Co-based catalysts, as shown in Fig. 4. Furthermore, the values of the rate constant of the FTS reaction do not vary with Ru particle size, which suggests that the particle size does not influence the intrinsic activity of the active sites on Ru-based catalysts. The authors proposed that the lower TOF value for small Ru nanoparticles (< 10 nm) might be related to strong adsorption of CO. A higher coverage of CO will therefore lead to a more difficult CO activation on smaller Ru nanoparticles. This Ru particle size effect is different than that found in Xiao's work [31], in which the FTS reaction occurred in the aqueous phase.

The different conclusions in these works dealing with the effect of Ru particle size may originate from the use of different supports. Our recent work [33] on an aqueous-phase FTS reaction over Ru-based catalysts shows that the TOF of FTS increases with particle size (1–5 nm), with a plateau between 2.3 nm and 3.7 nm. Small clusters will not have a step-edge site to dissociate CO, which reduces FTS activity. The chain growth parameter for hydrocarbon formation is not influenced when particles are larger than 2.5 nm.

2.3. Fe particle size effect in FTS

Iron is the cheapest transition metal for the fabrication of FTS catalysts. Iron carbides are generally considered for the active phase of FTS. It is well known that Fe-based catalysts present significantly high water-gas-shift ($CO + H_2O \longrightarrow CO_2 + H_2$) activity. Therefore, Fe can serve as a suitable FTS catalyst when the H_2/CO ratio is significantly lower than 2. Compared with Co, Fe has a lower methanation activity and a higher selectivity toward short hydrocarbon chains. The product slate obtained with Fe-based catalysts usually contains higher olefin content than that obtained with Co catalysts. Clarification of the optimal size of Fe-based catalysts with high activity and selectivity for desirable products is of continuing interest to the FTS community.

Previous experimental works showed that FTS activity and selectivity are closely related to the particle size of Fe-based catalysts. For example, Mabaso et al. [34] mentioned that catalysts containing Fe nanoparticles smaller than 7–9 nm present lower TOF and higher CH_4 selectivity than those containing larger particles. Olefin selectivity is not affected by particle size, whereas small Fe nanoparticles exhibit lower chain growth probability and higher CH_4 selectivity. These findings were confirmed by Liu et al. [35], who showed that smaller Fe nanoparticles generate more short-chain hydrocarbons including CH_4. Further investigation showed that the TOF increases when the Fe particle size increases from 2.4 nm to 6.2 nm, and then remains almost constant up to a particle size of 11.5 nm, as shown in Fig. 5 [36]. This set of Fe-based catalysts also presented an increase of CH_4 selectivity with decreasing particle size.

Torres Galvis et al. [12] studied the influence of iron carbide particle size using carbon nanofibers as a support. These catalysts showed deceasing activity with increasing particle size from 2 nm to 7 nm. However, the particle size of the Fe-based catalyst had no effect on olefin or CH_4 selectivity. In contrast to the unpromoted iron

carbide catalysts, the Na- and S-promoted catalysts showed quite different catalytic behavior. The TOF of CH_4 and C_{2+} formation as a function of particle size is shown in Fig. 6 [12]. It was found that CH_4 selectivity increases when the iron carbide particle size decreases from 7 nm to 2 nm. However, the selectivity of olefins is almost independent of iron carbide particle size. Smaller iron carbide particles display higher activity, mainly due to higher CH_4 production. The authors proposed that the corners and edges sites are quite important for CH_4 formation, while the terrace sites are feasible sites for olefins generation. A decrease of particle size results in more abundant step and edges sites, and ultimately in higher CH_4 production [12].

The results discussed above indicate that the catalytic activity of the FTS reaction is closely related to the particle size of Co-, Ru-, and Fe-based catalysts. Although the origin of the particle size effect is still controversial, the insights revealed are quite helpful for the rational design of highly efficient and stable catalysts with maximum mass-specific reactivity.

3. Effect of metal particle crystal phase in Fischer-Tropsch synthesis

Aside from the particle size effect, it has been found that FTS activity and selectivity depend on the crystal phase of the catalysts [37–56]. Catalysts with different crystal structures generally have distinct morphologies and surface topologies, which expose different concentrations of active sites that can result in very different catalytic performances. Here, we focus on recent works for Co-, Ru-, Fe-, and Ni-based catalysts.

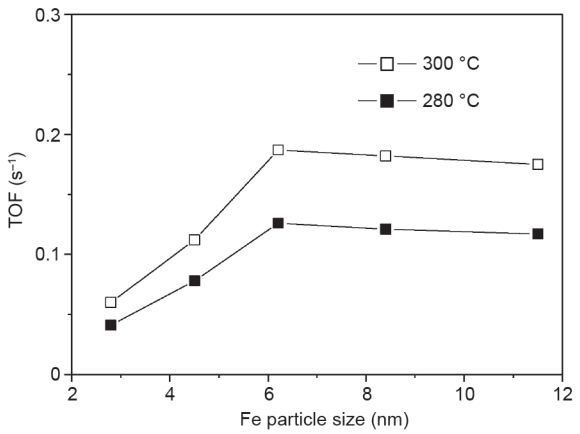

Fig. 5. The TOF of FTS as a function of Fe particle size with reaction temperatures of T = 280 °C and 300 °C [36].

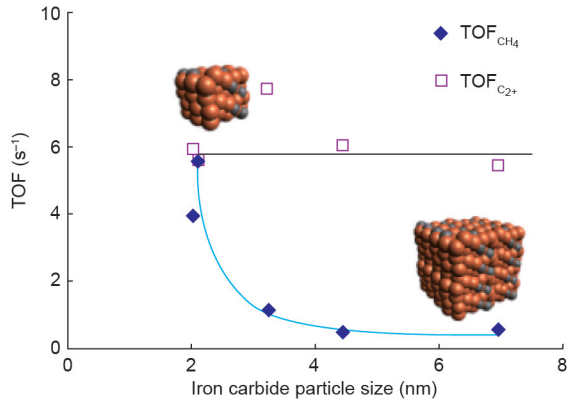

Fig. 6. Apparent TOF of CH_4 and C_{2+} hydrocarbons varying with iron carbide size (TOS = 1 h). The reaction was performed at 340 °C, 20 bar with H_2/CO = 1 on promoted catalysts [12]. TOS: time on-stream.

3.1. Co crystal phase effect in FTS

For Co, it is mostly assumed that metallic Co nanoparticles comprise the active phase in the FTS reaction. Bulk Co adopts a hexagonal close-packed (HCP) structure under ambient conditions. A temperature-induced phase transformation of HCP Co to the metastable face-centered cubic (FCC) Co occurs at 400 °C [57]. Such an HCP-to-FCC transformation has also been observed under much milder conditions when the Co particle size becomes very small. Specifically, HCP Co is the dominant phase when the particle size is above 40 nm, whereas the FCC lattice is adopted when Co nanoparticles are smaller than 20 nm [58]. Under FTS conditions, the actual crystal structure of metallic Co nanoparticles depends on the support type, the presence of promoters, and the particle size [58]. The pretreatment/activation of the catalyst will also affect this structure [59–61]. Such changes in crystal structure may play an important role in FTS activity and selectivity.

It has been reported by many groups that HCP Co exhibits higher FTS activity than FCC Co [37,44,45,50–52,62]. In particular, Ducreux et al. [45] reported that Co-based catalysts mainly consisting of HCP Co nanoparticles had higher FTS activity than catalysts containing predominantly FCC Co nanoparticles (Fig. 7(a)). Another work demonstrated that the FCC Co nanoparticle is less active than the HCP Co nanoparticle; the cobalt carbide (Co_2C) nanoparticle is inactive for FTS (Fig. 7(b)) [37]. Recently, Davis et al. [52] found that Co-based catalysts containing the HCP phase display higher CO conversion rates than FCC Co nanoparticles in FTS. Compared with FCC Co nanoparticles, HCP Co nanoparticles exhibit a slightly higher olefin selectivity in the C_2–C_4 hydrocarbon range and a lower rate of CH_4 formation. It is proposed that the higher conversion of CO on HCP Co

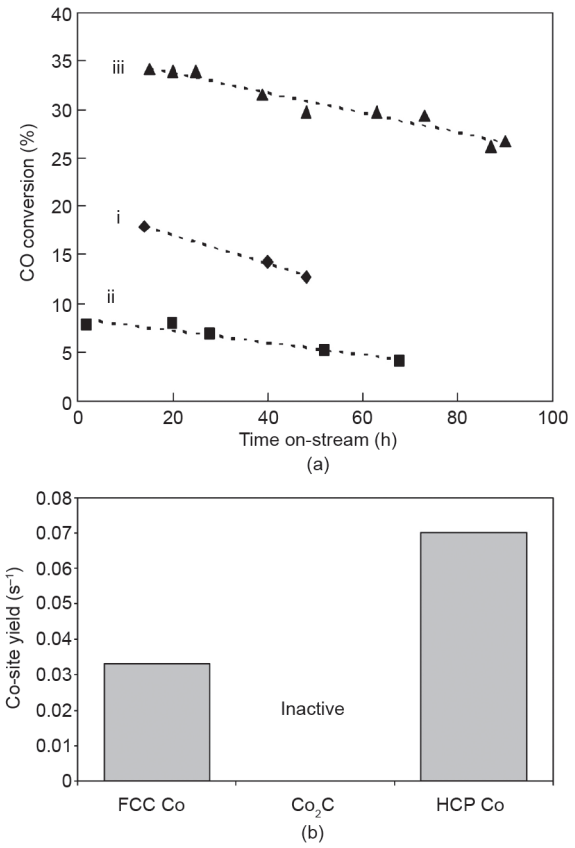

Fig. 7. (a) CO conversion as a function of time for a Co-Ru/SiO_2 catalyst: (i) mixture of FCC-HCP structures (diamonds), (ii) FCC structure (squares), and (iii) HCP structure (triangles) [45]; (b) Co-site yields in FTS on FCC Co-, HCP Co-, and Co_2C-based catalysts [37].

nanoparticles is probably due to a higher density of surface defects and stacking faults [45,51].

Despite many studies, it remains an open question why the HCP Co nanoparticle displays higher activity than the FCC Co nanoparticle. Liu et al. [39] compared CO activation on HCP and FCC Co nanoparticles by first principles density functional theory (DFT) calculations. The morphologies of HCP and FCC Co nanoparticles were approximated by the Wulff construction [63]. As seen in Fig. 8, HCP and FCC Co nanoparticles exhibit different morphologies. Based on computed CO activation barriers, CO dissociation rates were estimated using transition-state theory. A major conclusion of this study was that four facets on the HCP Co nanoparticle—namely, $(11\bar{2}1)$, $(10\bar{1}1)$, $(10\bar{1}2)$, and $(11\bar{2}0)$—exhibit higher CO dissociation rates than the most active FCC (100) surface on the FCC Co nanoparticle. The HCP Co nanoparticle shows higher CO dissociation activity than the FCC Co nanoparticle because of the presence of more numerous and more active B5 sites. It was further established that the CO activation reaction pathways are different for HCP and FCC Co phases; that is, CO prefers a direct dissociation pathway on HCP Co phases, whereas an H-assisted route is important on FCC Co phases. Even considering the H-assisted CO activation pathway, the HCP Co phase displays higher activity than the FCC Co phase.

It is widely accepted that Co_2C is inert in FTS [37]. However, Ding et al. [64,65] observed that aliphatic C_1–C_{18} α-alcohols could be generated from syngas (CO + H_2) by using Co-based catalysts supported on activated carbon. The formation of Co_2C during the FTS reaction may be the key to obtaining higher alcohols [4,56,66,67]. The generation of higher alcohols appears to require the coexistence of Co and Co_2C, possibly indicating that the interface between Co and Co_2C is the active site for the FTS reaction. To test this hypothesis, researchers performed DFT calculations to clarify the active site and reaction mechanism for higher alcohol formation on Co-based catalysts (Fig. 9) [55]. The calculations suggested that CO can adsorb on Co_2C, but that it does not dissociate at this location. The researchers therefore argued that this CO can result in a higher rate of CO insertion at the Co/Co_2C interface, resulting in more aldehydes that are subsequently hydrogenated to alcohols. The reaction barrier for CO insertion into a CH_2 intermediate at the Co/Co_2C interface is relatively low at 0.77 eV. This insight opens the possibility of fine-tuning product composition.

Recently, Zhong et al. [53] synthesized manganese (Mn)-promoted Co_2C nanoprisms exhibiting high FTS activity. Such Co_2C catalysts generated much more light olefins (C_2–C_4 hydrocarbons) at relatively low CH_4 selectivity under mild FTS reaction conditions (Fig. 10). Moreover, the Co_2C nanoprisms showed excellent stability in the first 15 h. This result is particularly surprising, because conventional spherical Co_2C nanocrystals exhibit extremely low activity for FTS. Transmission electron micrograph characterization and DFT calculations showed that the preferentially exposed (101) and (020) facets might present particular active sites for syngas conversion into olefins. This work provides a new way to design the next generation of highly efficient Fischer-Tropsch-to-olefins (FTO) catalysts.

3.2. Ru crystal phase effect in FTS

Ru nanoparticles are widely used in heterogeneous catalysis. There is a growing interest in the relationship between the crystal structure of Ru-based catalysts and their performance. Kusada et al. [40] have synthesized pure FCC Ru nanoparticle catalysts. It was found that CO oxidation activity was strongly dependent on the crystal structure and particle size of Ru-based catalysts. Above 3 nm, the traditional HCP Ru nanoparticles were less active than the FCC Ru nanoparticles. It was proposed that the higher activity of FCC Ru nanoparticles stems from the presence of abundant (111) facets that can easily be oxidized to RuO_2 (110), which is more active than metallic Ru in CO oxidation. Later, Gu et al. [42] synthesized Ru@Pt core-shell catalysts that had an FCC structure and were largely enclosed by (111) facets. This Ru@Pt core-shell catalyst is more active

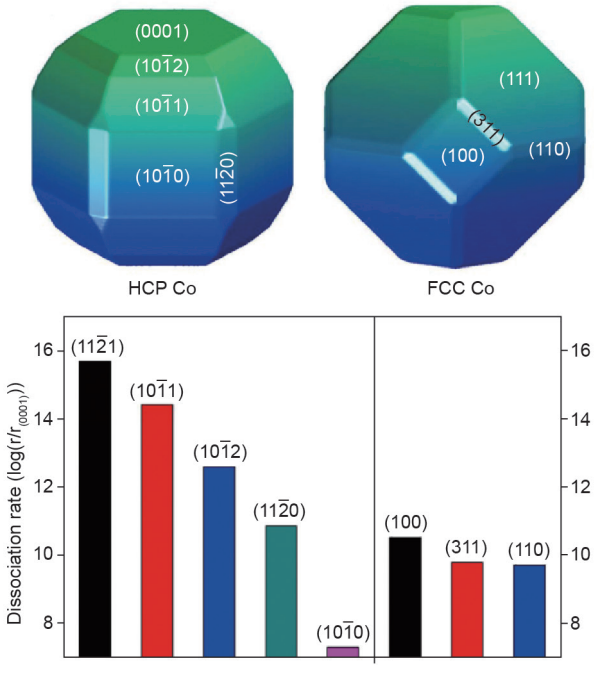

Fig. 8. Wulff shapes for HCP and FCC Co nanoparticles, and CO dissociation rates on the exposed HCP and FCC Co nanoparticle facets. All rates are normalized to that of HCP (0001) [39].

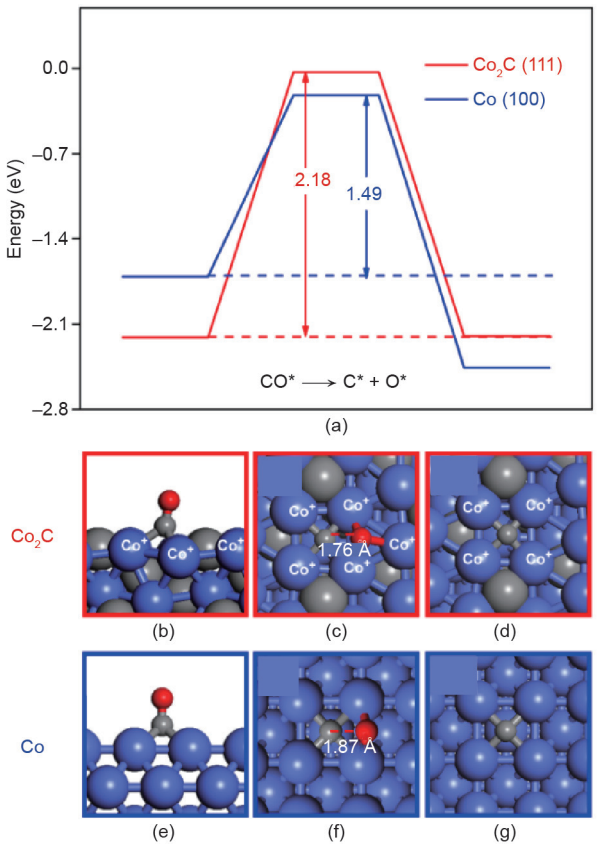

Fig. 9. The (a) potential energy surface and (b–g) geometric information of CO activation on Co_2C (111) (red) and Co (100) (blue) surfaces [55].

for the hydrogen evolution reaction than conventional HCP Ru catalysts [42]. Higher activity of FCC Ru nanoparticles than HCP Ru nanoparticles was also observed in other reactions, such as the conversion of ammonia-borane [48,68], the oxygen evolution reaction [69], hydrogenation reactions [70], and dinitrogen activation [71]. Thus, the question of how the FCC and HCP crystal structures of Ru-based catalysts impact the activity and selectivity of FTS remains an interesting and timely topic.

Li et al. [72] recently studied FTS on Ru-based catalysts with FCC and HCP structures by a combination of DFT calculations, modern materials synthesis, and scanning transmission electron microscope (STEM). DFT calculations showed that there are many open facets with modest CO dissociation barriers available on FCC Ru nanoparticle catalysts (Fig. 11), but only a few step edges with a lower barrier on HCP Ru nanoparticle catalysts. Based on these theoretical results, FCC Pt@Ru core-shell nanocrystal catalysts with high density of the active sites (open facets) were synthesized. The synthesized FCC Ru nanoparticle catalysts showed extraordinarily high specific activity in an aqueous-phase FTS process in the low temperature range of 393–433 K. The activity of FTS was as high as 37.8 $mol_{CO}·mol_{Ru}^{-1}·h^{-1}$ at 433 K, making this by far the most active FTS catalyst working at low temperatures (< 473 K). The origin of the high activity of FCC Ru nanoparticles stems from the higher active site density in comparison with HCP Ru nanoparticles. It is worth noting that the catalytic behavior trend between the HCP and FCC phase is dependent on the transition metals. For example, the FCC Co nanoparticle is less active than the HCP Co nanoparticle, whereas the Ru nanoparticle shows the opposite trend. The kinetic differences between Ru and Co nanoparticles in FTS mainly stem from these structural and electronic differences, which arise from the slightly larger lattice constant of the Ru nanoparticle.

3.3. Iron and iron carbides crystal phase effect in FTS

It is very difficult to synthesize pure iron carbide phases. The evolution of the active phase of Fe-based catalysts is very complicated, resulting in considerable debate on the nature of the active phase and on the FTS reaction mechanism for Fe-based catalysts. Understanding the phase distribution, phase evolution, and activity of different phases will accelerate the design of optimal Fe-based FTS catalysts. Different iron carbides, including ε-Fe_2C, ε′-$Fe_{2.2}C$, Fe_7C_3, χ-Fe_5C_2, and θ-Fe_3C, have been observed under FTS reaction conditions. Iron carbide phase transformation (ε–χ–θ phase transformation) will occur depending on the temperature and the H_2/CO ratio, as shown in Fig. 12 [73]. Specifically, the high temperature and low chemical potential of carbon (μ_C) (high H_2/CO ratio) generally result in preferential formation of θ-Fe_3C. In contrast, high μ_C (low H_2/CO ratio) and moderate temperature (~250 °C) lead to the formation of χ-Fe_5C_2. ε-carbides are preferentially formed at lower temperatures and even higher μ_C.

Identification of the active phase of iron carbides for FTS remains

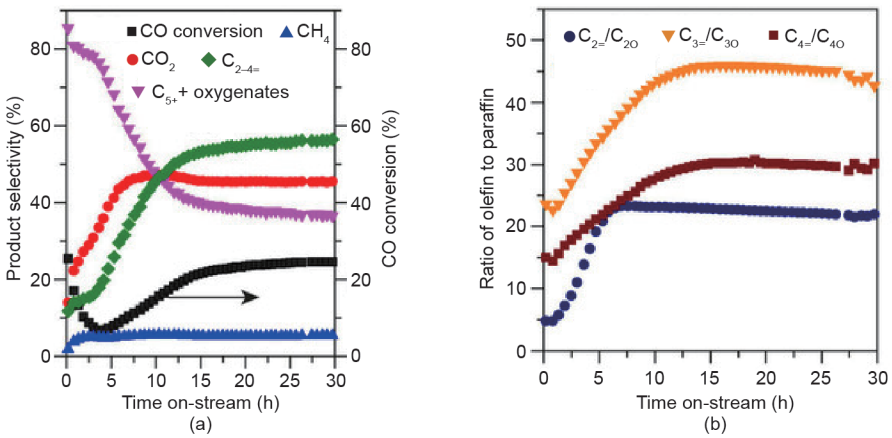

Fig. 10. Catalytic performance of the CoMn catalyst in the initial stages of the reaction. (a) CO conversion and product selectivity as a function of time on-stream; (b) ratio of olefin to paraffin as a function of time on-stream [53].

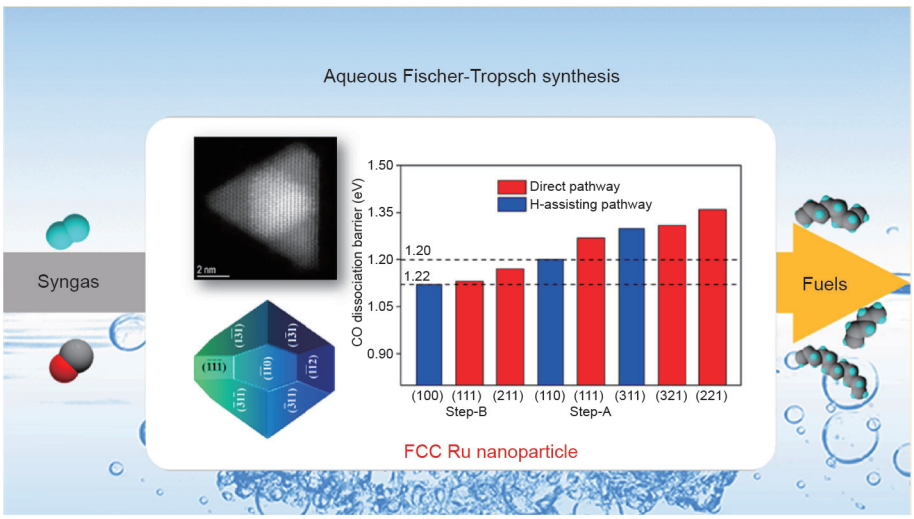

Fig. 11. Scheme for CO activation barriers on the facets of FCC Ru nanoparticle: Wulff construction and STEM image and modeled shapes of the synthesized Pt@Ru nanoparticles [72].

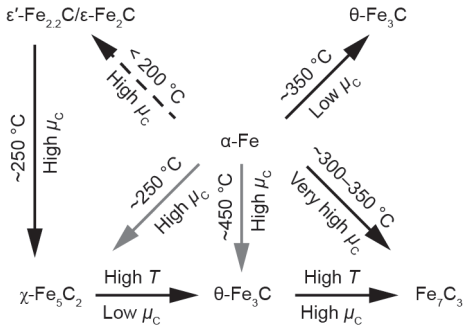

Fig. 12. Iron carbide phases varying with the temperature (T) and chemical potential of carbon [73].

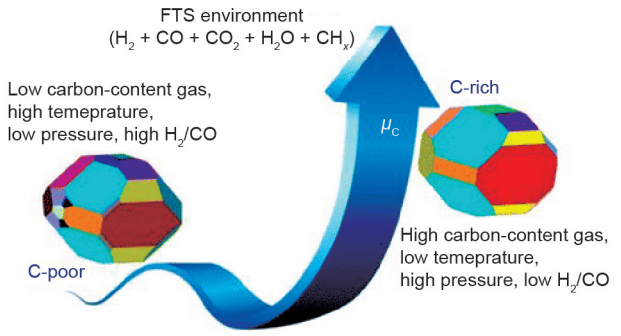

Fig. 13. The morphology of an Fe-based FTS catalyst varying under different reaction conditions [83].

a great challenge in heterogeneous catalysis. In fact, metallic iron [74,75] and various iron carbide phases have been claimed to be active for the FTS reaction [76–80]. De Smit et al. [73] reported that Fe-based catalysts mainly consist of χ-Fe_5C_2, which is active but prone to oxidation. On the other hand, θ-Fe_3C catalysts showed a lower activity and selectivity, which might be due to the buildup of carbonaceous deposits on the catalyst surface. This finding was confirmed by Fierro's experimental work showing that χ-Fe_5C_2 is more active than θ-Fe_3C catalysts for FTS [81]. Later, Yang et al. [82] first reported a facile wet chemical route for the synthesis of pure χ-Fe_5C_2 nanoparticles. These χ-Fe_5C_2 nanoparticle catalysts possess higher activity and selectivity than the conventional reduced-hematite catalysts.

Considering the temperature, pressure, and H_2/CO ratio effects, Zhao et al. [83] studied the surface structure and stability of various iron carbide phases (ε-Fe_2C, χ-Fe_5C_2, θ-Fe_3C, and Fe_4C) by DFT calculations (Fig. 13). Similar to De Smit's results [73], it was found that higher carbon-content gas always results in a higher carburization degree, which will be suppressed at higher temperature and lower pressure, and under higher H_2/CO ratio conditions. ε-Fe_2C, χ-Fe_5C_2, and θ-Fe_3C carbides result in different Wulff shapes. In general, the morphologies of iron carbides vary dramatically with the environment (H_2/CO ratio and temperature). By increasing the chemical potential of carbon, the most stable termination of the iron carbide surface changes to a carbon-rich surface with a high surface Fe/C ratio. Extensive CO activation has been studied on the obtained stable surfaces. CO adsorption and CH_4 formation is most feasible on χ-Fe_5C_2-(100)-2.25 termination, followed by θ-Fe_3C-(010)-2.33, ε-Fe_2C-(121)-2.00, and Fe_4C-(100)-3.00 termination, the latter of which has the lowest activity. The authors proposed that the different catalytic activities among different iron carbide phases may originate from the surface work function and charge state of the surface atoms [83]. Therefore, χ-Fe_5C_2 might be the most active phase for CO hydrogenation to CH_4.

Recently, Yang et al. [84] reported a ceria-supported subnanometer iron oxide cluster catalyst displaying high FTS activity. Using STEM and X-ray absorption fine structure (XAFS) characterizations, it was confirmed that the iron oxide clusters (Fe–O_x–Fe_y) containing partially reduced Fe^{d+} (d = 2.6–2.9) species in ceria nanorods are the active phase for FTS. Interestingly, these researchers did not observe any iron carbides for this catalyst during the FTS reaction. Their work indicates that the FTS activity is strongly related to the local coordination of the active site, and that iron carbides are not always the demanding phase for FTS. Although many studies have been performed, more experimental and theoretical work needs to be done to clarify the true active phase of Fe-based catalysts for FTS under realistic conditions.

3.4. Ni crystal phase effect in FTS

Nickel is not a good FTS catalyst because of its poor ability to dissociate CO, such that its use results predominantly in CH_4, and because of its instability, which is due to the formation of volatile carbonyls under practical FTS reaction conditions [85]. However, Ni can be used as an efficient catalyst for CH_4 production and as a promoter for FTS [86]. Bulk Ni adopts an FCC structure under ambient conditions. However, FCC Ni can transform into HCP Ni when the Ni particle size decreases to 4 nm [87]. In fact, HCP Ni nanoparticles have already been synthesized via a one-pot chemical route [87] and via other chemical methods [88–95]. It was found that HCP Ni nanoparticles have higher activity than FCC Ni nanoparticles in the aqueous-phase reforming of glycerol. Furthermore, HCP Ni nanoparticles can present higher H_2 selectivity and hinder CH_4 formation, compared with FCC Ni nanoparticles [96].

CO activation is the first crucial step in the CO methanation reaction. It is suggested that CO activation is closely related to the surface structures of Ni nanoparticles, and that under-coordinated step/edge sites are the active sites for CO dissociation [97,98]. CO activation via a COH intermediate is proposed to be the rate-determining step during CO methanation [99,100]. Liu et al. [54] performed DFT calculations to study the influence of the Ni crystal phase on CO activation (Fig. 14). Their computational analysis indicated that CO dissociation is strongly dependent on the crystal structure and morphology of Ni catalysts. It is important to note that CO dissociation assisted by hydrogen is kinetically favored over a direct dissociation pathway, irrespective of the crystal phases. As seen in Fig. 14, (311) and $(10\bar{1}2)$ are the most active facets for FCC Ni and HCP Ni, respectively. CO dissociation prefers the COH intermediate on the most active surface of FCC and HCP Ni catalysts. FCC Ni is more active than HCP Ni because FCC Ni can expose abundant facets with low activation barriers. The distinct behaviors of different crystal phases (FCC versus HCP) revealed here are valuable for catalyst optimization to expose abundant active sites for activating diatomic molecules.

4. Conclusions and perspective

The identification of the relationship between structures and the catalytic activity of the FTS reaction will accelerate optimal catalyst design. In this paper, we summarized recent progress on the dependence of the FTS performance on particle size and crystal phase effects. FTS activity and selectivity strongly depend on the particle size of the catalysts. However, the origin of the particle size in FTS remains controversial due to the high complexity of the FTS reaction mechanism and to limitations of *in situ* characterizations. Catalysts with different crystal phases and structures have different morphologies; the resulting different electronic states result in substantial activity and selectivity variations. It is more necessary than ever to develop modern characterization techniques and advanced material synthesis methodologies, and to combine these with DFT

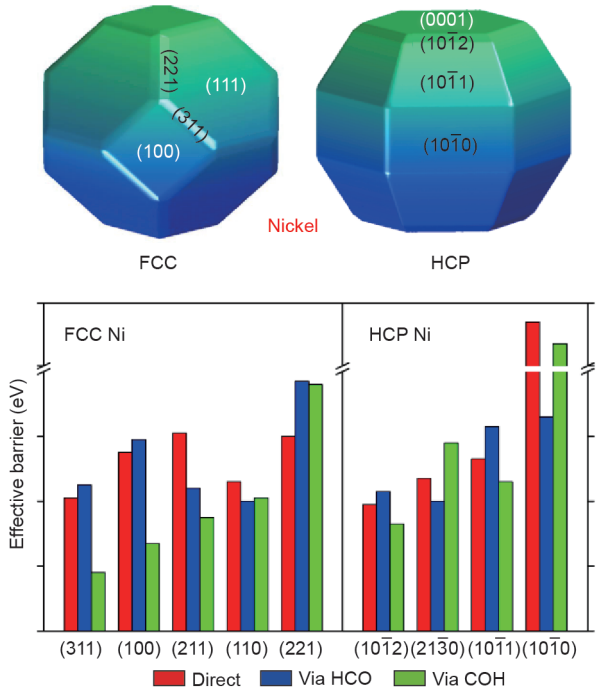

Fig. 14. CO activation on FCC and HCP Ni morphologies, obtained by Wulff construction [54].

calculations applied to model and technical catalyst systems, in order to identify active sites and explore novel concepts that can dramatically improve the performance of metallic catalysts in the hydrogenation of CO to chemicals and fuels.

Acknowledgements

We acknowledge financial support by NWO-VICI and NWO-TOP grants awarded to Emiel J. M. Hensen.

Compliance with ethics guidelines

Jin-Xun Liu, Peng Wang, Wayne Xu, and Emiel J. M. Hensen declare that they have no conflict of interest or financial conflicts to disclose.

References

[1] Schulz H. Short history and present trends of Fischer–Tropsch synthesis. Appl Catal A Gen 1999;186(1–2):3–12.
[2] Baliban RC, Elia JA, Weekman V, Floudas CA. Process synthesis of hybrid coal, biomass, and natural gas to liquids via Fischer–Tropsch synthesis, ZSM-5 catalytic conversion, methanol synthesis, methanol-to-gasoline, and methanol-to-olefins/distillate technologies. Comput Chem Eng 2012;47:29–56.
[3] Fischer F, Tropsch H. The preparation of synthetic oil mixtures (synthol) from carbon monoxide and hydrogen. Brennstoff Chem 1923;4:276–85.
[4] Filot IAW, van Santen RA, Hensen EJM. The optimally performing Fischer–Tropsch catalyst. Angew Chem 2014;126(47):12960–4. German.
[5] Nørskov JK, Bligaard T, Rossmeisl J, Christensen CH. Towards the computational design of solid catalysts. Nat Chem 2009;1(1):37–46.
[6] Zhou K, Li Y. Catalysis based on nanocrystals with well-defined facets. Angew Chem Int Ed 2012;51(3):602–13.
[7] Den Breejen JP, Radstake PB, Bezemer GL, Bitter JH, Frøseth V, Holmen A, et al. On the origin of the cobalt particle size effects in Fischer–Tropsch catalysis. J Am Chem Soc 2009;131(20):7197–203.
[8] Fu Q, Li WX, Yao Y, Liu H, Su HY, Ma D, et al. Interface-confined ferrous centers for catalytic oxidation. Science 2010;328(5982):1141–4.
[9] Huo CF, Wu BS, Gao P, Yang Y, Li YW, Jiao H. The mechanism of potassium promoter: Enhancing the stability of active surfaces. Angew Chem Int Ed 2011;50(32):7403–6.
[10] Jacobs G, Das TK, Zhang Y, Li J, Racoillet G, Davis BH. Fischer–Tropsch synthesis: Support, loading, and promoter effects on the reducibility of cobalt catalysts. Appl Catal A Gen 2002;233(1–2):263–81.
[11] Van Santen RA. Complementary structure sensitive and insensitive catalytic relationships. Acc Chem Res 2009;42(1):57–66.
[12] Torres Galvis HM, Bitter JH, Davidian T, Ruitenbeek M, Dugulan AI, de Jong KP. Iron particle size effects for direct production of lower olefins from synthesis gas. J Am Chem Soc 2012;134(39):16207–15.
[13] Enger BC, Holmen A. Nickel and Fischer–Tropsch synthesis. Catal Rev 2012;54(4):437–88.
[14] Valden M. Onset of catalytic activity of gold clusters on titania with the appearance of nonmetallic properties. Science 1998;281(5383):1647–50.
[15] Bezemer GL, Bitter JH, Kuipers HP, Oosterbeek H, Holewijn JE, Xu X, et al. Cobalt particle size effects in the Fischer–Tropsch reaction studied with carbon nanofiber supported catalysts. J Am Chem Soc 2006;128(12):3956–64.
[16] Carballo JMG, Yang J, Holmen A, García-Rodríguez S, Rojas S, Ojeda M, et al. Catalytic effects of ruthenium particle size on the Fischer–Tropsch synthesis. J Catal 2011;284(1):102–8.
[17] Kellner CS, Bell AT. Effects of dispersion on the activity and selectivity of alumina-supported ruthenium catalysts for carbon monoxide hydrogenation. J Catal 1982;75(2):251–61.
[18] Iglesia E. Design, synthesis, and use of cobalt-based Fischer–Tropsch synthesis catalysts. Appl Catal A Gen 1997;161(1–2):59–78.
[19] Wang Z, Skiles S, Yang F, Yan Z, Goodman DW. Particle size effects in Fischer–Tropsch synthesis by cobalt. Catal Today 2012;181(1):75–81.
[20] Prieto G, Martínez A, Concepción P, Moreno-Tost R. Cobalt particle size effects in Fischer–Tropsch synthesis: Structural and *in situ* spectroscopic characterisation on reverse micelle-synthesised Co/ITQ-2 model catalysts. J Catal 2009;266(1):129–44.
[21] Herranz T, Deng X, Cabot A, Guo J, Salmeron M. Influence of the cobalt particle size in the CO hydrogenation reaction studied by *in situ* X-ray absorption spectroscopy. J Phys Chem B 2009;113(31):10721–7.
[22] Tuxen A, Carenco S, Chintapalli M, Chuang CH, Escudero C, Pach E, et al. Size-dependent dissociation of carbon monoxide on cobalt nanoparticles. J Am Chem Soc 2013;135(6):2273–8.
[23] Yang J, Tveten EZ, Chen D, Holmen A. Understanding the effect of cobalt particle size on Fischer–Tropsch synthesis: Surface species and mechanistic studies by SSITKA and kinetic isotope effect. Langmuir 2010;26(21):16558–67.
[24] Borg Ø, Dietzel PD, Spjelkavik AI, Tveten EZ, Walmsley JC, Diplas S, et al. Fischer–Tropsch synthesis: Cobalt particle size and support effects on intrinsic activity and product distribution. J Catal 2008;259(2):161–4.
[25] Rane S, Borg Ø, Rytter E, Holmen A. Relation between hydrocarbon selectivity and cobalt particle size for alumina supported cobalt Fischer–Tropsch catalysts. Appl Catal A Gen 2012;437–8:10–7.
[26] Melaet G, Lindeman AE, Somorjai GA. Cobalt particle size effects in the Fischer–Tropsch synthesis and in the hydrogenation of CO_2 studied with nanoparticle model catalysts on silica. Top Catal 2014;57(6–9):500–7.
[27] Dalla Betta RA, Piken AG, Shelef M. Heterogeneous methanation: Initial rate of CO hydrogenation on supported ruthenium and nickel. J Catal 1974;35(1):54–60.
[28] Iglesia E, Soled SL, Fiato RA. Fischer–Tropsch synthesis on cobalt and ruthenium. Metal dispersion and support effects on reaction rate and selectivity. J Catal 1992;137(1):212–24.
[29] Smith KJ, Everson RC. Fischer–Tropsch reaction studies with supported ruthenium catalysts: II. Effects of oxidative pretreatment at elevated temperatures. J Catal 1986;99(2):349–57.
[30] Kang J, Zhang S, Zhang Q, Wang Y. Ruthenium nanoparticles supported on carbon nanotubes as efficient catalysts for selective conversion of synthesis gas to diesel fuel. Angew Chem 2009;121(14):2603–6. German.
[31] Xiao C, Cai Z, Wang T, Kou Y, Yan N. Aqueous-phase Fischer–Tropsch synthesis with a ruthenium nanocluster catalyst. Angew Chem 2008;120(4):758–61. German.
[32] Quek XY, Guan Y, van Santen RA, Hensen EJ. Unprecedented oxygenate selectivity in aqueous-phase Fischer–Tropsch synthesis by ruthenium nanoparticles. ChemCatChem 2011;3(11):1735–8.
[33] Quek XY, Pestman R, van Santen RA, Hensen EJ. Structure sensitivity in the ruthenium nanoparticle catalyzed aqueous-phase Fischer–Tropsch reaction. Catal Sci Technol 2014;4(10):3510–23.
[34] Mabaso EI, van Steen E, Claeys M. Fischer–Tropsch synthesis on supported iron crystallites of different size. In: Proceedings of the DGMK/SCI-Conference "Synthesis Gas Chemistry"; 2006 Oct 4–6; Dresden, Germany. 2006. p. 93–100.
[35] Liu Y, Chen JF, Zhang Y. The effect of pore size or iron particle size on the formation of light olefins in Fischer–Tropsch synthesis. RSC Advances 2015;5(37):29002–7.
[36] Park JY, Lee YJ, Khanna PK, Jun KW, Bae JW, Kim YH. Alumina-supported iron oxide nanoparticles as Fischer–Tropsch catalysts: Effect of particle size of iron oxide. J Mol Catal Chem 2010;323(1–2):84–90.
[37] Sadeqzadeh M, Karaca H, Safonova O, Fongarland P, Chambrey S, Roussel P, et al. Identification of the active species in the working alumina-supported cobalt catalyst under various conditions of Fischer–Tropsch synthesis. Catal Today 2011;164(1):62–7.
[38] Mou X, Zhang B, Li Y, Yao L, Wei X, Su DS, et al. Rod-shaped Fe_2O_3 as an efficient catalyst for the selective reduction of nitrogen oxide by ammonia. Angew Chem Int Ed 2012;51(12):2989–93.
[39] Liu J, Su H, Sun D, Zhang B, Li W. Crystallographic dependence of CO activation

on cobalt catalysts: HCP versus FCC. J Am Chem Soc 2013;135(44):16284–7.
[40] Kusada K, Kobayashi H, Yamamoto T, Matsumura S, Sumi N, Sato K, et al. Discovery of face-centered cubic ruthenium nanoparticles: Facile size-controlled synthesis using the chemical reduction method. J Am Chem Soc 2013;135(15):5493–6.
[41] Jin H, Lee KW, Khi NT, An H, Park J, Baik H, et al. Rational synthesis of heterostructured M/Pt (M = Ru or Rh) octahedral nanoboxes and octapods and their structure-dependent electrochemical activity toward the oxygen evolution reaction. Small 2015;11(35):4462–8.
[42] Gu J, Guo Y, Jiang Y, Zhu W, Xu Y, Zhao Z, et al. Robust phase control through hetero-seeded epitaxial growth for face-centered cubic Pt@Ru nanotetrahedrons with superior hydrogen electro-oxidation activity. J Phys Chem C 2015;119(31):17697–706.
[43] Liu J, Li W. Theoretical study of crystal phase effect in heterogeneous catalysis. WIREs Comput Mol Sci 2016;6(5):571–83.
[44] Ducreux O, Lynch J, Rebours B, Roy M, Chaumette P. *In situ* characterisation of cobalt based Fischer-Tropsch catalysts: A new approach to the active phase. In: Fornasiero P, Cargnello M, editors Morphological, compositional, and shape control of materials for catalysis. Amsterdam: Elsevier; 1998. p. 125–30.
[45] Ducreux O, Rebours B, Lynch J, Roy-Auberger M, Bazin D. Microstructure of supported cobalt Fischer-Tropsch catalysts. Oil Gas Sci Technol 2009;64(1):49–62.
[46] Guo Y, Liu X, Azmat MU, Xu W, Ren J, Wang Y, et al. Hydrogen production by aqueous-phase reforming of glycerol over Ni-B catalysts. Int J Hydrogen Energy 2012;37(1):227–34.
[47] Song C, Sakata O, Kumara LSR, Kohara S, Yang A, Kusada K, et al. Size dependence of structural parameters in FCC and HCP Ru nanoparticles, revealed by Rietveld refinement analysis of high-energy X-ray diffraction data. Sci Rep 2016;6(1):31400.
[48] Ma H, Na C. Isokinetic temperature and size-controlled activation of ruthenium-catalyzed ammonia borane hydrolysis. ACS Catal 2015;5(3):1726–35.
[49] Fan Z, Zhang H. Crystal phase-controlled synthesis, properties and applications of noble metal nanomaterials. Chem Soc Rev 2016;45(1):63–82.
[50] De la Peña O'Shea VA, Homs N, Fierro JLG, Ramírez de la Piscina P. Structural changes and activation treatment in a Co/SiO_2 catalyst for Fischer–Tropsch synthesis. Catal Today 2006;114(4):422–7.
[51] Enache DI, Rebours B, Roy-Auberger M, Revel R. *In situ* XRD study of the influence of thermal treatment on the characteristics and the catalytic properties of cobalt-based Fischer–Tropsch catalysts. J Catal 2002;205(2):346–53.
[52] Gnanamani MK, Jacobs G, Shafer WD, Davis BH. Fischer–Tropsch synthesis: Activity of metallic phases of cobalt supported on silica. Catal Today 2013;215:13–7.
[53] Zhong L, Yu F, An Y, Zhao Y, Sun Y, Li Z, et al. Cobalt carbide nanoprisms for direct production of lower olefins from syngas. Nature 2016;538(7623):84–7.
[54] Liu J, Zhang B, Chen P, Su H, Li W. CO dissociation on face-centered cubic and hexagonal close-packed nickel catalysts: A first-principles study. J Phys Chem C 2016;120(43):24895–903.
[55] Pei Y, Liu J, Zhao Y, Ding Y, Liu T, Dong W, et al. High alcohols synthesis via Fischer–Tropsch reaction at cobalt metal/carbide interface. ACS Catal 2015;5(6):3620–4.
[56] Dong W, Liu J, Zhu H, Ding Y, Pei Y, Liu J, et al. $Co–Co_2C$ and $Co–Co_2C$/AC catalysts for hydroformylation of 1-hexene under low pressure: Experimental and theoretical studies. J Phys Chem C 2014;118(33):19114–22.
[57] Hansen M, Anderko K. Constitution of binary alloys. 1st ed. Elliot RP, editor. New York: McGraw-Hill Book Company; 1965.
[58] Kitakami O, Sato H, Shimada Y, Sato F, Tanaka M. Size effect on the crystal phase of cobalt fine particles. Phys Rev B 1997;56(21):13849–54.
[59] Fischer N, van Steen E, Claeys M. Preparation of supported nano-sized cobalt oxide and FCC cobalt crystallites. Catal Today 2011;171(1):174–9.
[60] Braconnier L, Landrivon E, Clémençon I, Legens C, Diehl F, Schuurman Y. How does activation affect the cobalt crystallographic structure? An *in situ* XRD and magnetic study. Catal Today 2013;215:18–23.
[61] Prieto G, Concepción P, Murciano R, Martínez A. The impact of pre-reduction thermal history on the metal surface topology and site-catalytic activity of Co/SiO_2 Fischer–Tropsch catalysts. J Catal 2013;302:37–48.
[62] Karaca H, Safonova OV, Chambrey S, Fongarland P, Roussel P, Griboval-Constant A, et al. Structure and catalytic performance of Pt-promoted alumina-supported cobalt catalysts under realistic conditions of Fischer–Tropsch synthesis. J Catal 2011;277(1):14–26.
[63] Wulff G. Zur frage der geschwindigkeit des wachsthums und der auflösung der krystallflächen. Zeitschrift Kristallographie Mineralogie 1901;34(1–6):449–530. German.
[64] Ding Y, Zhu H, Wang T, Jiao G, Lu Y. Process for directly producing mixed linear α-alcohols having 1 to 18 carbon atoms from synthesis gas. United States patent US 7468396. 2008 Dec 23.
[65] Ding Y, Zhu H, Wang T, Jiao G, Lu Y. Activated carbon supported cobalt based catalyst for directly converting of synthesis gas to mixed linear α-alcohols and paraffins. United States patent US 7670985. 2010 Mar 2.
[66] Volkova GG, Yurieva TM, Plyasova LM, Naumova MI, Zaikovskii V. Role of the Cu–Co alloy and cobalt carbide in higher alcohol synthesis. J Mol Catal Chem 2000;158(1):389–93.
[67] Lebarbier VM, Mei D, Kim DH, Andersen A, Male JL, Holladay JE, et al. Effects of La_2O_3 on the mixed higher alcohols synthesis from syngas over Co catalysts: A combined theoretical and experimental study. J Phys Chem C 2011;115(35):17440–51.
[68] Abo-Hamed EK, Pennycook T, Vaynzof Y, Toprakcioglu C, Koutsioubas A, Scherman OA. Highly active metastable ruthenium nanoparticles for hydrogen production through the catalytic hydrolysis of ammonia borane. Small 2014;10(15):3145–52.
[69] AlYami NM, LaGrow AP, Joya KS, Hwang J, Katsiev K, Anjum DH, et al. Tailoring ruthenium exposure to enhance the performance of FCC platinum@ruthenium core-shell electrocatalysts in the oxygen evolution reaction. Phys Chem Chem Phys 2016;18(24):16169–78.
[70] Yao Y, He DS, Lin Y, Feng X, Wang X, Yin P, et al. Modulating FCC and hcp ruthenium on the surface of palladium–copper alloy through tunable lattice mismatch. Angew Chem 2016;128(18):5591–5. German.
[71] Zhao M, Figueroa-Cosme L, Elnabawy AO, Vara M, Yang X, Roling LT, et al. Synthesis and characterization of Ru cubic nanocages with a face-centered cubic structure by templating with Pd nanocubes. Nano Lett 2016;16(8):5310–7.
[72] Li W, Liu J, Gu J, Zhou W, Yao S, Si R, et al. Chemical insights into the design and development of face-centered cubic ruthenium catalysts for Fischer–Tropsch synthesis. J Am Chem Soc 2017;139(6):2267–76.
[73] De Smit E, Cinquini F, Beale AM, Safonova OV, van Beek W, Sautet P, et al. Stability and reactivity of ε-χ-θ iron carbide catalyst phases in Fischer–Tropsch synthesis: Controlling μ_c. J Am Chem Soc 2010;132(42):14928–41.
[74] Niemantsverdriet JW, van der Kraan AM, van Dijk WM, van der Baan HS. Behavior of metallic iron catalysts during Fischer–Tropsch synthesis studied with Mössbauer spectroscopy, X-ray diffraction, carbon content determination, and reaction kinetic measurements. J Phys Chem 1980;84(25):3363–70.
[75] Kuei CK, Lee MD. Temperature-programmed reaction of pre-adsorbed CO on iron catalyst: New experimental evidence for competition model. J Mol Catal 1991;65(3):293–305.
[76] Bukur DB, Nowicki L, Manne RK, Lang X. Activation studies with a precipitated iron catalyst for Fischer–Tropsch synthesis: II. Reaction studies. J Catal 1995;155(2):366–75.
[77] Amelse JA, Butt JB, Schwartz LH. Carburization of supported iron synthesis catalysts. J Phys Chem 1978;82(5):558–63.
[78] Bukur DB, Okabe K, Rosynek MP, Li C, Wang D, Rao K, et al. Activation studies with a precipitated iron catalyst for Fischer–Tropsch synthesis: I. Characterization studies. J Catal 1995;155(2):353–65.
[79] Badani MV, Delgass WN. The active phase of iron catalysts for acetonitrile synthesis. J Catal 1999;187(2):506–17.
[80] Mansker LD, Jin Y, Bukur DB, Datye AK. Characterization of slurry phase iron catalysts for Fischer–Tropsch synthesis. Appl Catal A Gen 1999;186(1–2):277–96.
[81] Herranz T, Rojas S, Pérez-Alonso FJ, Ojeda M, Terreros P, Fierro JLG. Genesis of iron carbides and their role in the synthesis of hydrocarbons from synthesis gas. J Catal 2006;243(1):199–211.
[82] Yang C, Zhao H, Hou Y, Ma D. Fe_5C_2 nanoparticles: A facile bromide-induced synthesis and as an active phase for Fischer–Tropsch synthesis. J Am Chem Soc 2012;134(38):15814–21.
[83] Zhao S, Liu X, Huo C, Li Y, Wang J, Jiao H. Determining surface structure and stability of ε-Fe_2C, χ-Fe_5C_2, θ-Fe_3C and Fe_4C phases under carburization environment from combined DFT and atomistic thermodynamic studies. Catal Struct React 2015;1(1):44–60.
[84] Yang Q, Fu X, Jia C, Ma C, Wang X, Zeng J, et al. Structural determination of catalytically active subnanometer iron oxide clusters. ACS Catal 2016;6(5):3072–82.
[85] Dry M. FT catalysts. In: Steynberg A, Dry M, editors Fischer–Tropsch technology. Amsterdam: Elsevier; 2004. p. 533–600.
[86] Rytter E, Skagseth TH, Eri S, Sjåstad AO. Cobalt Fischer–Tropsch catalysts using nickel promoter as a rhenium substitute to suppress deactivation. Ind Eng Chem Res 2010;49(9):4140–8.
[87] Illy S, Tillement O, Machizaud F, Dubois J, Massicot F, Fort Y, et al. First direct evidence of size-dependent structural transition in nanosized nickel particles. Philos Mag A 1999;79(5):1021–31.
[88] Hemenger P, Weik H. On the existence of hexagonal nickel. Acta Cryst 1965;19:690–1.
[89] Mi Y, Yuan D, Liu Y, Zhang J, Xiao Y. Synthesis of hexagonal close-packed nanocrystalline nickel by a thermal reduction process. Mater Chem Phys 2005;89(2–3):359–61.
[90] Han M, Liu Q, He J, Song Y, Xu Z, Zhu J. Controllable synthesis and magnetic properties of cubic and hexagonal phase nickel nanocrystals. Adv Mater 2007;19(8):1096–100.
[91] Lahiri A, Das R. Synthesis of face-centered cubic and hexagonal closed-packed nickel using ionic liquids. J Appl Electrochem 2010;40(11):1991–5.
[92] Lahiri A, Das R, Reddy RG. Electrochemical synthesis of hexagonal closed-pack nickel: A hydrogen storage material. J Power Sources 2010;195(6):1688–90.
[93] Lahiri A, Tadisina Z. Synthesis, thermodynamic and magnetic properties of pure hexagonal close-packed nickel. Mater Chem Phys 2010;124(1):41–3.
[94] Bolokang AS, Phasha MJ. Novel synthesis of metastable HCP nickel by water quenching. Mater Lett 2011;65(1):59–60.
[95] Kotoulas A, Gjoka M, Simeonidis K, Tsiaoussis I, Angelakeris M, Kalogirou O, et al. The role of synthetic parameters in the magnetic behavior of relative large HCP Ni nanoparticles. J Nanopart Res 2011;13(5):1897–908.
[96] Guo Y, Azmat MU, Liu X, Ren J, Wang Y, Lu G. Controllable synthesis of hexagonal close-packed nickel nanoparticles under high nickel concentration and its catalytic properties. J Mater Sci 2011;46(13):4606–13.
[97] Bengaard H, Nørskov JK, Sehested J, Clausen BS, Nielsen LP, Molenbroek AM, et al. Steam reforming and graphite formation on Ni catalysts. J Catal

2002;209(2):365–84.
[98] Engbæk J, Lytken O, Nielsen JH, Chorkendorff I. CO dissociation on Ni: The effect of steps and of nickel carbonyl. Surf Sci 2008;602(3):733–43.
[99] Van Ho S, Harriott P. The kinetics of methanation on nickel catalysts. J Catal 1980;64(2):272–83.
[100] Andersson MP, Abild-Pedersen F, Remediakis IN, Bligaard T, Jones G, Engbæk J, et al. Structure sensitivity of the methanation reaction: H_2-induced CO dissociation on nickel surfaces. J Catal 2008;255(1):6–19.